In-situ reflection imaging and microspectroscopic study on three-dimensional crystal growth of L-phenylalanine under laser trapping

Jim Jui-Kai Chen[1], Ken-ichi Yuyama[1,2]*, Teruki Sugiyama[1,3,4]*, and Hiroshi Masuhara[1,3]*

[1]*Department of Applied Chemistry, National Chiao Tung University, Hsinchu 30010, Taiwan*
[2]*Research Institute for Electronic Science, Hokkaido University, Sapporo, Hokkaido 001-0020, Japan*
[3]*Center for Emergent Functional Matter Science, National Chiao Tung University, Hsinchu 30010, Taiwan*
[4]*Division of Materials Science, Graduate School of Science and Technology, Nara Institute of Science and Technology, Ikoma, Nara 630-0192, Japan*

E-mail: yuyama@es.hokudai.ac.jp, sugiyama@g2.nctu.edu.tw, masuhara@masuhara.jp

We investigated growth behavior of an L-phenylalanine crystal formed by laser trapping with the use of reflection imaging and microspectroscopy. Optical reflection micrographs show colored images of the crystal due to constructive interference of incident white light. The color distribution on the crystal is dynamically changed under laser trapping, which is in addition to enlargement of the crystal plane area. The temporal change in the crystal thickness is examined by measuring reflection spectra of the crystal. We discuss the three-dimensional crystal growth under laser trapping condition by comprehensively considering the changes in the crystal thickness and the crystal plane area.

Ashkin *et al.* demonstrated optical trapping with the use of a tightly focused laser beam in 1986.[1] Since then, it has been widely used as optical tweezers capable of trapping and manipulating small objects in solution.[2] In particular, optical tweezers have played an innovative role in biological research by non-contact and invasive manipulation of microorganisms and organelles.[3–5] For objects much smaller than the wavelength of the laser, many of the objects are simultaneously confined in the focal volume, forming their assembly. This assembly formation was demonstrated for plasmonic nanoparticles[6–8], polymeric nanospheres[9], semiconductor quantum dots[10,11], polymers[12–14], proteins[15–17], and amino acids[18].

Assembly formation by laser trapping was extended to spatio-temporal control of crystallization. In 2007, we demonstrated, for the first time, laser trapping-induced crystallization for glycine, which was achieved by focusing a continuous-wave (cw) laser beam at the air/solution interface of the supersaturated D_2O solution.[19] After that, the crystallization was extended to other amino acids[20,21], sodium chlorate[22], and hybrid perovskite compounds[23,24]. It is worth noting that the crystallization is induced even in unsaturated solution, and only one single crystal is formed from the focal spot. By taking these advantages, we investigated growth behavior of single L-phenylalanine (L-Phe) crystal under various laser trapping and solution conditions.[21] We measured its two-dimensional (2D) growth rate with transmission imaging and found that the rate is controllable in the unsaturated solutions by changing laser power. However, no information on crystal thickness was obtained with the transmission imaging.

In this work, we have applied reflection imaging and microspectroscopy to investigate the change in thickness of a single L-Phe crystal prepared by laser trapping at the air/solution interface. Namely, white light was introduced to the L-Phe crystal under laser trapping condition, and constructive interference of the white light reflected at the lower and upper crystal faces was observed. Colorful crystal images were obtained in the reflection imaging, and thickness distribution in the crystal was visualized. In addition, the temporal change in the crystal thickness was examined by measuring reflection spectra of the crystal using a detector coupled with a spectrograph. We discuss the three-dimensional (3D) crystal growth behavior under laser trapping condition by comprehensively considering the changes in the crystal thickness and the crystal plane area.

Upon focusing a cw laser beam (λ = 1064 nm) at the air/solution interface of the L-Phe aqueous solution (saturation degree: 0.58), crystallization of the plate-like anhydrous form was induced from the focal spot. The details of sample preparation and optical setup are described in Supporting Information (SI). It was reported that a plate-shaped anhydrous crystal of L-Phe is stable at temperatures above 37°C.[25] On the other hand, needle-like monohydrate crystals are formed below this transition temperature. Under the present irradiation conditions, local temperature elevation over 20 K is induced concurrently with laser trapping.[26] This laser heating is caused by 1064-nm light absorption mainly of solvent H_2O molecules. Cooperative phenomena of concentration increase of L-Phe and temperature elevation lead to the formation of a supersaturated region of which temperature is over the transition point. As a result, nucleation of a plate-shaped anhydrous crystal of L-Phe is triggered at the focal spot.

Figure 1a shows a series of reflection images of an L-Phe crystal after the nucleation. The images were obtained under laser irradiation to the crystal central part. The crystal was stably trapped by the laser and continuously grew to a larger size. A video of this growth behavior can be seen in SI. Different from transmission imaging, a colored crystal was observed in the optical reflection micrographs. The coloration results from constructive interference of the white light reflected at the lower and upper crystal faces as an L-Phe crystal has no absorption at the examined wavelength. The crystal was mainly colored as green and purple. This is due to the transmittance of a dichromatic mirror, because the white light reflected at the crystal is detected with the imaging camera after passing through the dichromatic mirror.

It should be noted that the color was different depending on the position on the crystal. It seemed that the color is extended from the focus toward its outside in a cross shape, implying that the crystal thickness is not homogeneous and has spatial distribution. We consider that the area observed as the cross shape in Fig. 1a is thick compared to the other parts of the crystal. Furthermore, the color distribution was dynamically changed, which was in addition to enlargement of the crystal plane area. This result indicates that the L-Phe crystal increases in its thickness as well as its plane area under laser irradiation into the crystal central part.

Figure 1b shows the temporal change in the crystal plane area for the sample of Fig. 1a.

The temporal change can be fitted with a linear function. Here, we defined crystallization time (T_{cryst}) and 2D crystal growth rate ($R_{lateral\text{-}2D}$) as follows. T_{cryst} was calculated as an intersection between the fitted linear function and the x-axis. The slope of the fitted linear function was deemed as $R_{lateral\text{-}2D}$. In this sample, T_{cryst} and $R_{lateral\text{-}2D}$ were estimated at 494 sec and 8.8 μm^2/sec, respectively. T_{cryst} was much different among samples and distributed at 200–800 sec even under the same solution and irradiation conditions. The variation of T_{cryst} is probably due to the stochastic nature of a nucleation phenomenon, as one single crystal is always formed and monitored. Different from laser trapping-induced crystallization, single femtosecond laser pulse immediately triggers crystal nucleation through the formation and collapse of a cavitation bubble.[27] Therefore, femtosecond laser irradiation might be useful to control T_{cryst} under laser trapping condition. As shown in Fig. 1c, $R_{lateral\text{-}2D}$ became faster with the increase in T_{cryst}. Namely, an L-Phe crystal taking longer time for nucleation grows at a faster speed. This tendency was the same as that for the higher concentration L-Phe solutions with a saturation degree of 0.67–0.92.[21] This is because a cluster domain is formed prior to nucleation, and its concentration is increased with time. Since the crystal is formed and grown in the cluster domain under the laser irradiation, $R_{lateral\text{-}2D}$ becomes faster with the increase in T_{cryst}.

Here, we discuss the mechanism of the 2D growth laterally proceeding along the solution surface from the optical viewpoint that was proposed in our previous papers.[21,28] The laser irradiated into the crystal central part is guided to the crystal edge and generates optical potential there. Due to this potential, L-Phe molecules/clusters in the cluster domain are attracted to the crystal, and the crystal continues to grow even in unsaturated solution. In fact, a nanoparticle assembly sticking out a chain-like structure is formed upon laser trapping of 500-nm polystyrene nanoparticles at the glass/solution interface.[29] The chain-like structure confining nanoparticles one-dimensionally is generated as the result of outward light scattering/propagation from the laser focus. We infer that the thicker crystal part with the cross shape in Fig. 1a has the role in guiding the focused laser up to the crystal edge, similar to the case of the chain-like structure of nanoparticles.[29] At the present stage, we consider that the geometrical relation between the laser polarization and L-Phe clusters and the birefringent character of the crystal may determine the propagation direction of the trapping laser, giving the cross shape.

The coloration of the crystal in the optical reflection images is ascribed to constructive interference of incident white light. The constructive interference is induced in accordance with the following equation;

$$2 \cdot n \cdot d \cdot \cos(\theta) = \left(m - \frac{1}{2}\right) \cdot \lambda, \qquad (m = 1, 2, \cdots)$$

, where n is the refractive index of the L-Phe crystal, d is the crystal thickness, and θ is the refraction angle of the incident light inside the crystal. Constructive interference occurs at the wavelength of λ. Assuming that the refractive index (n) and the refraction angle (θ) are constant during laser trapping, the peak positions in reflection spectra shift depending only on the crystal thickness (d). A reflection band shifts to long wavelength with the increase in the crystal thickness.

We measured reflection spectra under the microscope and calculated crystal thickness on the basis of the above principle. Figure 2a shows the temporal change in the reflection spectra during the laser irradiation into the crystal central part. The time after starting the spectroscopic measurement is shown in the graph. In the beginning, two reflection bands were observed around 520 and 650 nm, which was followed by red-shift of these reflection bands. They kept shifting to longer wavelength with time under the laser trapping condition. Finally, one of them moved to the wavelength longer than 750 nm, which is the detection limit of the current optical system. After 15 sec, a new reflection band appeared at 470 nm and red-shifted with time. At the present optical setup, θ has distribution, leading to the decrease in amplitude of reflection spectra. In the case that white light is irradiated perpendicular to the crystal, spectral bandwidth becomes narrow, and the number of reflection bands is increased, which will make spectral analysis easier. We will construct a new optical setup to realize such illumination condition in the near future.

We calculated the crystal thickness from the peak positions of the reflection spectra by assuming n = 1.6[30] and θ = 25[31]. Figure 2b shows its time evolution during the laser trapping. The crystal thickness was increased linearly with time. The slope can be deemed as the growth rate in the crystal thickness ($R_{thickness}$), which was estimated at 5.5 nm/sec for this sample. Figure 2c shows the temporal change in the crystal thickness upon decreasing the laser power in a step-by-step manner from 1.1 to 0.5 W. The laser power and $R_{thickness}$ are shown in the graph. The initial $R_{thickness}$ at 1.1 W was 14.7 nm/sec, and it slowed down to 8.9 nm/sec at 0.8 W and attained 5.4 nm/sec at 0.5 W. This tendency upon the decrease in the

laser power was summarized in Fig. 2d for 4 samples, in which $R_{thickness}$ was normalized with the rate at 1.1 W in each sample. The variation of $R_{thickness}$ among samples at each laser power is possibly ascribed to solution concentration around the crystal that fluctuates during 2D crystal growth. Thus, $R_{thickness}$ is controllable by laser power, similarly to the control of $R_{lateral-2D}$ reported in the previous work.[21)]

For discussing the dynamics of the crystal growth perpendicular and parallel to the solution surface, we plotted $R_{thickness}$ against T_{cryst} in Fig. 3a. The result showed that $R_{thickness}$ has less correlation to T_{cryst}. This trend was different from that between $R_{lateral-2D}$ and T_{cryst} (Fig. 1c). Actually, $R_{thickness}$ and $R_{lateral-2D}$ likely have less relationship with each other, which is shown in Fig. 3b. This result implies that the lateral growth and the thickness increase independently proceed with different mechanism.

In order to compare the lateral growth and the thickness increase with the same unit (nm/sec), we calculate one-dimensional rate [$R_{lateral-1D}$ (nm/sec)] for the crystal growth parallel to the solution surface. For the calculation, we assume that the shape of an L-Phe crystal is in a square shape and each side with the length of $r(t)$ grows at the rate of $R_{lateral-1D}(t)$ (inset of Fig. 4a). The beginning of t corresponds to T_{cryst}. Since the plane area of an L-Phe crystal is enlarged linearly with time at the rate of $R_{lateral-2D}$, the crystal plane area at a certain time can be expressed as $r(t)^2 = R_{lateral-2D} \cdot t$. The increment of the crystal plane area is approximately shown as $R_{lateral-2D} \approx 4 \cdot r(t) \cdot R_{lateral-1D}(t)$. Based on these relations, it can be calculated that $R_{lateral-1D}(t)$ is proportional to $(R_{lateral-2D}/t)^{0.5}$. $R_{lateral-1D}(t)$ is decreased as the function of $t^{-0.5}$, as schematically illustrated in Fig. 4a. On the other hand, the crystal thickness is increased linearly with time (Fig. 2b), and $R_{thickness}$ is constant independent of time (Fig. 4b). Thus, $R_{lateral-1D}$ and $R_{thickness}$ have a different tendency for their temporal changes, but $R_{lateral-1D}$ should be much fast than $R_{thickness}$, considering the plate shape of the crystal.

Based on the above consideration, the possible dynamics of the 3D crystal growth under laser trapping is shown in Fig. 5. Upon the laser irradiation into the air/solution interface, a cluster domain is formed prior to nucleation (Fig. 5a). Subsequently, crystal nucleation is induced stochastically at the focal spot in the cluster domain (Fig. 5b). Since the concentration of the cluster domain is increased with time,[21)] $R_{lateral-2D}$ becomes faster for the sample of longer T_{cryst}. The mechanism of 2D crystal growth can be explained from the

optical viewpoint. The laser irradiated into the crystal central part propagates to the crystal edge, and the optical force is generated there. It is reasonable to consider that the laser intensity at the crystal edge becomes weak with the increase in the propagation length. Accordingly, trapping efficiency at the crystal edge is decreased with the enlargement of the crystal plane area. As a result, the one-dimensional growth rate parallel to the solution surface ($R_{lateral\text{-}1D}$) becomes slow with time (Fig. 5c–5d).

On the other hand, the one-dimensional growth rate perpendicular to the solution surface ($R_{thickness}$) is constant independent of time. At the focal spot where reflection spectra were obtained, the optical force is directly generated by the focused laser beam. Therefore, optical force is always exerted to L-Phe, and L-Phe is continuously supplied to the focal spot. As a result, $R_{thickness}$ is kept constant against irradiation time (Fig. 5c–5d). Due to continuous laser trapping of L-Phe, $R_{thickness}$ might be less influenced by the concentration of the cluster domain, in other words, T_{cryst}. The crystal thickness at the focal spot should be thick compared to the surrounding area. Such crystal morphology is possibly helpful for the trapping laser to be efficiently confined in the crystal and guided outwardly to the crystal edge.

In conclusion, we applied reflection imaging and microspectroscopy to laser trapping-induced crystallization of L-Phe. The rate of the crystal growth perpendicular to the solution surface is constant during laser irradiation. On the other hand, the one-dimensional growth rate parallel to the solution surface becomes slow with time. We explained these behaviors by considering optical force exerted directly by the focused laser to the crystal surface, and that generated at the crystal edge through light propagation inside the crystal. We believe that these new insights are helpful to understand laser trapping-induced crystallization and useful to design new experiments on the precise control of crystal growth with the use of spatially modified laser beams.

Acknowledgments

The present work is partly supported by the Center for Emergent Functional Matter Science of National Chiao Tung University from The Featured Areas Research Center Program within the framework of the Higher Education SPROUT Project by the Ministry of Education (MOE) in Taiwan. Thanks are also due to the Ministry of Science and Technology

(MOST) in Taiwan (MOST 108-2113-M-009-011- to T.S. and MOST 108-2113M-009-015- to H.M.) and JSPS KAKENHI Grant Number JP16H06507 in Scientific Research on Innovative Areas “Nano-Material Optical-Manipulation” to T.S.

References

1) A. Ashkin, J. M. Dziedzic, J. E. Bjorkholm, and S. Chu, Opt. Lett. **11**, 288 (1986).
2) A. Ashkin, Proc. Natl. Acad. Sci. USA **94**, 4853 (1997).
3) A. Ashkin, J. M. Dziedzic, and T. Yamane, Nature **330**, 769 (1987).
4) A. Ashkin, and J. M. Dziedzic, Science **235**, 1517 (1987).
5) A. Ashkin, K. Schütze, J. M. Dziedzic, U. Euteneuer, and M. Schliwa, Nature **348**, 346 (1990).
6) H. Yoshikawa, T. Matsui, and H. Masuhara, Phys. Rev. E **70**, 061406 (2004).
7) Y. Tanaka, H. Yoshikawa, T. Itoh, and M. Ishikawa, Opt. Express **17**, 18760 (2009).
8) A. Ohlinger, S. Nedev, A. A. Lutich, and J. Feldmann, Nano Lett. **11**, 1770 (2011).
9) C. Hosokawa, H. Yoshikawa, and H. Masuhara, Phys. Rev. E **70**, 061410 (2004).
10) L. Pan, A. Ishikawa, and N. Tamai, Phys. Rev. B **75**, 161305(R) (2007).
11) W.-Y. Chiang, T. Okuhata, A. Usman, N. Tamai, and H. Masuhara, J. Phys. Chem. B **1183**, 14010 (2014).
12) J. Hofkens, J. Hotta, K. Sasaki, H. Masuhara, and K. Iwai, Langmuir **13**, 414 (1997).
13) T. Shoji, R. Nohara, N. Kitamura, and Y. Tsuboi, Anal. Chim. Acta 854**75**, 118 (2015).
14) W. Singer, T. A. Nieminen, N. R. Heckenberg, and H. Rubinsztein-Dunlop, Phys. Rev. E **75**, 011916 (2007).
15) Y. Tsuboi, T. Shoji, and N. Kitamura, Jpn. J. Appl. Phys. **46**, L1234 (2007).
16) Y. Tsuboi, T. Shoji, M. Nishino, S. Masuda, K. Ishimori, and N. Kitamura, Appl. Surf. Sci. **255**, 9906 (2009).
17) T. Shoji, N. Kitamura, and Y. Tsuboi, J. Phys. Chem. C **117**, 10691 (2013).
18) Y. Tsuboi, T. Shoji, and N. Kitamura, J. Phys. Chem. C **114**, 5589 (2010).
19) T. Sugiyama, T. Adachi, and H. Masuhara, Chem. Lett. **36**, 1480 (2007).
20) K. Yuyama, K. Ishiguro, T. Sugiyama, and H. Masuhara, Proc. SPIE **8458**, 84582D-1 (2014).
21) K. Yuyama, J. George, K. G. Thomas, T. Sugiyama, and H. Masuhara, Cryst. Growth Des.

16, 953 (2016).

22) H. Niinomi, T. Sugiyama, K. Miyamoto, and T. Omatsu, Cryst. Growth Des. **18**, 734 (2018).

23) K. Yuyama, Md J. Islam, K. Takahashi, T. Nakamura, and V. Biju, Angew. Chem. Int. Ed. **57**, 13424 (2018).

24) Md J. Islam, K. Yuyama, K. Takahashi, T. Nakamura, K. Konishi, and V. Biju, NPG Asia Mater. **11**, 31 (2019).

25) R. Mohan, K.-K. Koo, C. Strege, and A. S. Myerson, Ind. Eng. Chem. Res. **40**, 6111 (2001).

26) S. Ito, T. Sugiyama, N. Toitani, G. Katayama, and H. Miyasaka, J. Phys. Chem. B **111**, 2365 (2007).

27) K. Nakamura, Y. Hosokawa, and H. Masuhara, Cryst. Growth Des. **7**, 885 (2007).

28) K. Yuyama, T. Sugiyama, and H. Masuhara, J. Phys. Chem. Lett. **4**, 2436 (2013).

29) T. Kudo, S.-F. Wang, K. Yuyama, and H. Masuhara, Nano Lett. **16**, 3058 (2016).

30) M. A. Hernandez-Perez, C. Garapon, C. Champeaux, and J. C. Orlianges, J. Phys. Conf. Ser. **59**, 724 (2007).

31) S.-F. Wang, K. Yuyama, T. Sugiyama, and H. Masuhara, J. Phys. Chem. C **120**, 15578 (2016).

Figure Captions

Fig. 1. (a) Optical reflection micrographs of an L-Phe plate-like crystal under laser trapping condition. The irradiation time is shown in each image. The power of the laser after passing through the objective lens was 1.1 W. (b) The temporal change in the crystal plane area. (c) The plot of $R_{lateral\text{-}2D}$ against T_{cryst} for 21 samples.

Fig. 2. The temporal changes in (a) reflection spectra and (b) estimated crystal thickness of an L-Phe plate-like crystal under laser trapping condition. (c) The time evolution of thickness of an L-Phe crystal upon decreasing the laser power from 1.1 to 0.5 W in a step-by-step manner. (d) The change in the crystal thickness upon the step-by-step decrease in laser power. $R_{thickness}$ was normalized with the rate at 1.1 W in each sample.

Fig. 3. The relations of (a) $R_{thickness}$ and T_{cryst} and (d) $R_{thickness}$ and $R_{lateral\text{-}2D}$.

Fig. 4. Temporal change tendencies of (a) $R_{lateral\text{-}1D}$ and (b) $R_{thickness}$.

Fig. 5. Schematic illustration of the 3D growth dynamics of an L-Phe plate-shaped anhydrous crystal under laser trapping condition.

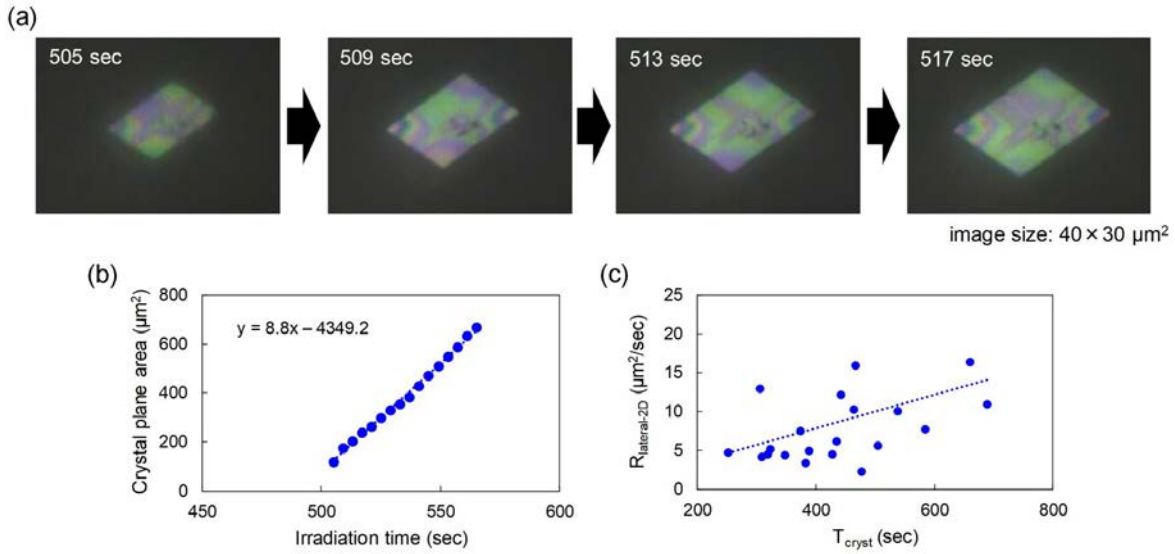

Fig.1. (a) Optical reflection micrographs of an L-Phe plate-like crystal under laser trapping condition. The irradiation time is shown in each image. The power of the laser after passing through the objective lens was 1.1 W. (b) The temporal change in the crystal plane area. (c) The plot of $R_{lateral\text{-}2D}$ against T_{cryst} for 21 samples.

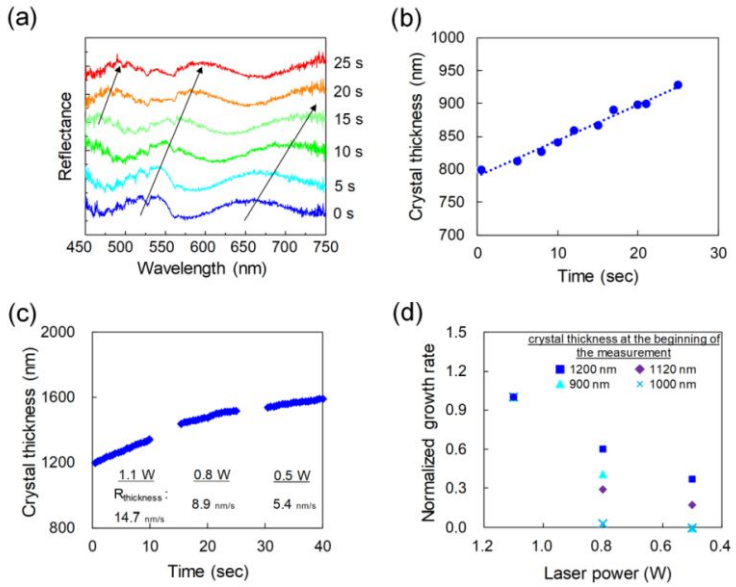

Fig. 2. The temporal changes in (a) reflection spectra and (b) estimated crystal thickness of an L-Phe plate-like crystal under laser trapping condition. (c) The time evolution of thickness of an L-Phe crystal upon decreasing the laser power from 1.1 to 0.5 W in a step-by-step manner. (d) The change in the crystal thickness upon the step-by-step decrease in laser power. $R_{thickness}$ was normalized with the rate at 1.1 W in each sample.

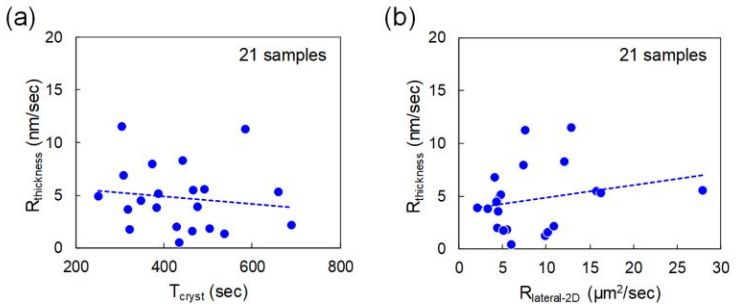

Fig. 3. The relations of (a) $R_{thickness}$ and T_{cryst} and (d) $R_{thickness}$ and $R_{lateral-2D}$.

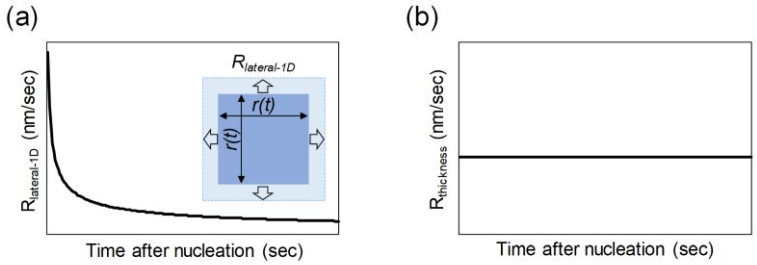

Fig. 4. Temporal change tendencies of (a) $R_{lateral\text{-}1D}$ and (b) $R_{thickness}$.

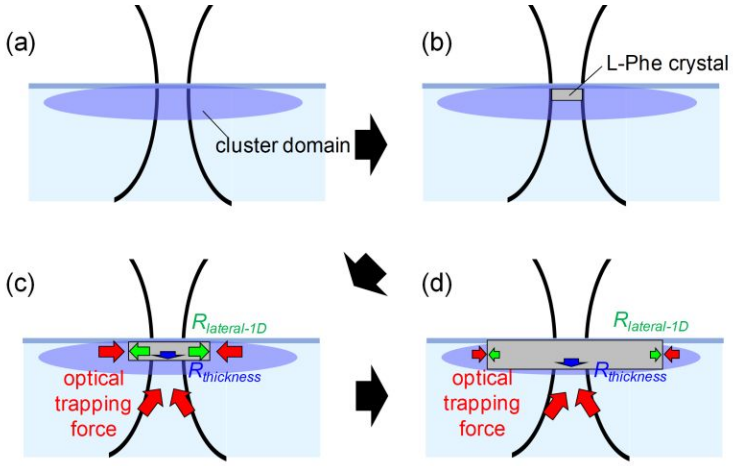

Fig. 5. Schematic illustration of the 3D growth dynamics of an L-Phe plate-shaped anhydrous crystal under laser trapping condition.